

Recoherence in the entanglement dynamics and classical orbits in the N -atom Jaynes-Cummings model

R. M. Angelo⁽¹⁾, K. Furuya⁽¹⁾, M. C. Nemes⁽²⁾, and G. Q. Pellegrino⁽³⁾

⁽¹⁾ *Instituto de Física “Gleb Wataghin”, Universidade Estadual de Campinas
13083-970 Campinas – SP, Brasil*

⁽²⁾ *Departamento de Física – ICEx, Universidade Federal de Minas Gerais
31270-901 Belo Horizonte – MG, Brasil*

⁽³⁾ *Departamento de Matemática, Universidade Federal de São Carlos
13560-970 São Carlos – SP, Brasil*

October 25, 2018

Abstract

The rise in linear entropy of a subsystem in the N -atom Jaynes-Cummings model is shown to be strongly influenced by the **shape** of the classical orbits of the underlying classical phase space: we find a one-to-one correspondence between maxima (minima) of the linear entropy and maxima (minima) of the expectation value of atomic excitation J_z . Since the expectation value of this operator can be viewed as related to the orbit radius in the classical phase space projection associated to the atomic degree of freedom, the proximity of the quantum wave packet to this atomic phase space borderline produces a maximum rate of entanglement. The consequence of this fact for initial conditions centered at periodic orbits in regular regions is a clear periodic recoherence. For chaotic situations the same phenomenon (proximity of the atomic phase space borderline) is in general responsible for oscillations in the entanglement properties.

PACS numbers: 05.45.Mt, 32.80.Qk

I INTRODUCTION

The importance of studying in detail the decoherence process is twofold. Firstly it may be viewed as a key to the understanding of some of the striking differences between the quantum and classical description of the world such as “the non existence at the classical level of the majority of states allowed by quantum mechanics” [1]. The decoherence process is believed to be the agent which eliminates interference between two or more macroscopically separated localized states [2]. Secondly, given the impressive technological advances in several experimental areas (Quantum Optics, Condensed Matter and Atomic Physics, etc.), it is nowadays possible to realize a system of two interacting degrees of freedom and watch the time evolution of the corresponding entanglement process [3]. It is therefore also of importance to understand the entanglement process in simple Hamiltonian systems. Two degrees of freedom Hamiltonian systems often present a very rich dynamics which in many cases is not yet completely understood from a general point of view. In particular, if the interaction is nonlinear the system may present chaotic behavior in the classical limit. The consequences of this fact to the quantum dynamics is yet an unsettled issue. A step in this direction was taken a few years ago, as it was conjectured that “the rate of entropy production can be used as an intrinsically quantum test of the chaotic versus regular nature of the evolution” [4]. The idea has been tested in some models [5, 6]. More specifically, in the context of the N -atom Jaynes-Cummings model, the reduced density linear entropy (or idempotency defect) has been used as a measure of the entanglement of the quantum subsystems. For a given classical energy, initial conditions for the quantum states are prepared as coherent wave packets centered at regular and chaotic regions of the classical phase space. For short times, a fast increase in decoherence for chaotic initial conditions is found when compared to regular ones. Typically the linear entropy in this model rises from zero to a plateau.

In the present contribution we show that this rise is strongly influenced by the **shape** of the atomic projection of classical orbits. There is a clear correlation between the rate of increase of linear entropy and the increase of the expectation value of the atomic excitation $\langle J_z \rangle(t)$ for short enough times. In classical terms, this can be visualized as follows: $\langle J_z \rangle(t)$ is a measure of the instantaneous radius of the projection of the trajectory in the atomic phase space. This atomic phase space is limited, the maximum radius corresponds to $\sqrt{4J} = \sqrt{2N}$, meaning therefore that the maximum rate

of entanglement can be directly associated to the proximity of this borderline. If the quantum evolution is such that the initial wave packet is centered at a classically regular region of the atomic phase space, in particular on a (non circular!) periodic orbit, the phenomenon is most conspicuous: as a function of time, the wave packet exhibits partial recoherences, well marked oscillations in the linear entropy superimposed to a steady increase, which can be immediately associated to smallest and largest distances from the classical border (largest or smallest $\langle J_z \rangle(t)$). If, on the other hand, the initial wave packet is centered on a classically chaotic region of the phase space, the recoherence phenomenon is of course not necessarily periodic in general. However we still find a connection between maxima and minima of the rate of linear entropy and $\langle J_z \rangle(t)$. As to be expected, this simple relation becomes less clear as quantum effects set in; in particular, for the chaotic region this happens much faster than for the regular one in a mixed phase space. Such effects are most marked at sufficiently long times, when a plateau in the linear entropy is reached. We show that at these times the spin projection of the wave packet becomes totally delocalized in phase space. This takes place for initial conditions centered at regular **and** chaotic regions, the regular cases taking longer times to achieve this delocalization.

In section II we present the model and the technical tools to be used in the following sections to analyze the entanglement property, connecting it to the classical regularity and chaos in a mixed regimen. Section III is devoted to the presentation of analysis and results in regular regions, whereas section IV deals with chaotic regions. A summary is given in section V.

II THE MODEL

We consider the N -atom Jaynes-Cummings model [7] whose Hamiltonian is given by

$$H = \hbar\omega_0 a^\dagger a + \varepsilon J_z + \frac{G}{\sqrt{2J}} (aJ_+ + a^\dagger J_-) + \frac{G'}{\sqrt{2J}} (a^\dagger J_+ + aJ_-) \quad (1)$$

where the first term corresponds to the energy of the free single-mode quantized field with frequency ω_0 , described by the creation (annihilation) operators a^\dagger (a); the second term corresponds to the energy of the $N = 2J$ two-level atoms with energy separation $\hbar\varepsilon$, and the operators J_z , $J_\pm = J_x \pm iJ_y$ are the usual angular momentum ones corresponding to the group $SU(2)$.

These operators satisfy the well known commutation relations:

$$\begin{aligned} [a, a^\dagger] &= 1, \\ [J_i, J_j] &= i\hbar J_k \end{aligned}$$

with the indices (i, j, k) forming any cyclic permutation of (x, y, z) . The last two terms in eq. (1) represent the interaction energy between the atomic system and the single-mode field.

The above Hamiltonian is a generalized version of the usual N -atom Jaynes-Cummings model to which we have added a Counter-Rotating Wave (CRW) term, with coupling constant G' . The so-called Rotating Wave Approximation (RWA) has been much in use for the proposals of mesoscopic superpositions of collective atomic states [8, 9] and in the generation of multiparticle entangled states in cavity QED experiments [10].

The N -atom JCM can also be realized in systems where trapped ions interact with laser fields. In that situation the bosonic operators a and a^\dagger describe the vibrational motion of the ions in the trap. Recently, reversible entanglement of ions has been proposed [11], and experimental realizations have been reported in the cases of two and four ions [12], with possible extensions to several ions [13]. In the trapped-ion system there is the possibility of generating both RW and CRW types of interaction by means of either a bichromatic laser excitation — with both G and G' different from zero — or appropriate excitation modes [14]. In the latter case, there would be the possibility to test the effects of RW ($G' = 0$) and CRW ($G = 0$) terms separately or together.

In our model we also add the supposition that the two coupling constants can be independently varied. When one of the coupling constants G or G' is set to zero, we have an integrable system. For $G' = 0$ ($G = 0$) there is an additional conserved quantity, namely the total excitation $P = J_z/\hbar + a^\dagger a$ (the relative excitation $P' = J_z/\hbar - a^\dagger a$). The system is otherwise nonintegrable and known to exhibit chaotic behavior in the classical limit [15]. In both cases, the quantum dynamics will produce entanglement, due to the coupling terms. This essentially quantum property can be quantified, e.g. by means of the linear entropy (or idempotency defect) associated to the reduced density matrices of the atomic or field subsystems (from this point on we shall set $\hbar = 1$),

$$\delta(t) = 1 - \text{Tr}_i(\rho_i(t)^2), \quad (2)$$

where

$$\rho_i(t) = Tr_j (|\psi(t)\rangle \langle\psi(t)|) \quad (3)$$

(i and j stand for the atomic and field subsystems, $i \neq j$). The quantities expressed in eqs. (2) and (3) are to be calculated using quantum states evolving in time under the action of Hamiltonian (1). To this end, the initial conditions chosen in the present study are such that

$$|\psi(0)\rangle = |w\rangle \otimes |v\rangle \equiv |wv\rangle \quad (4)$$

where $|w\rangle$ ($|v\rangle$) are atomic (field) coherent states given by [16]

$$|w\rangle = (1 + w\bar{w})^{-J} e^{wJ_+} |J, -J\rangle \quad (5)$$

$$|v\rangle = e^{-v\bar{v}/2} e^{vb^\dagger} |0\rangle \quad (6)$$

with

$$w = \frac{p_a + iq_a}{\sqrt{4J - (p_a^2 + q_a^2)}}, \quad (7)$$

$$v = \frac{1}{\sqrt{2}} (p_f + iq_f); \quad (8)$$

$|J, -J\rangle$ being the state with spin J and $J_z = -J$, $|0\rangle$ being the harmonic oscillator ground state, and p_a, q_a, p_f, q_f describing the phase space of the system into consideration. Generation of atomic coherent states in N -atom systems has been proposed in [8] and analyzed in [9].

The classical Hamiltonian corresponding to eq. (1) can be obtained by a standard procedure as [17]

$$\mathcal{H}(v, v^*, w, w^*) \equiv \langle wv | H | wv \rangle. \quad (9)$$

$\mathcal{H}(v, v^*, w, w^*)$ can be rewritten in terms of the phase space variables, reading

$$\begin{aligned} \mathcal{H}(q_a, p_a, q_f, p_f) &= \frac{\omega_0}{2} (p_f^2 + q_f^2) + \frac{\varepsilon}{2} (p_a^2 + q_a^2 - 2J) + \\ &+ \sqrt{1 - \frac{p_a^2 + q_a^2}{4J}} (G_+ p_a p_f + G_- q_a q_f), \end{aligned} \quad (10)$$

where $G_\pm = G \pm G'$.

The corresponding equations of motion are then given by

$$\begin{aligned}
\dot{q}_a &= -\frac{\partial \mathcal{H}}{\partial p_a} = -\varepsilon p_a - G_+ p_f \sqrt{1 - \frac{q_a^2 + p_a^2}{4J}} + \frac{p_a}{\sqrt{4J}} \frac{(G_+ p_a p_f + G_- q_a q_f)}{\sqrt{4J - (q_a^2 + p_a^2)}} \\
\dot{q}_f &= -\frac{\partial \mathcal{H}}{\partial p_f} = -\omega_0 p_f - G_+ p_a \sqrt{1 - \frac{q_a^2 + p_a^2}{4J}} \\
\dot{p}_a &= \frac{\partial \mathcal{H}}{\partial q_a} = \varepsilon q_a + G_- q_f \sqrt{1 - \frac{q_a^2 + p_a^2}{4J}} - \frac{q_a}{\sqrt{4J}} \frac{(G_+ p_a p_f + G_- q_a q_f)}{\sqrt{4J - (q_a^2 + p_a^2)}} \\
\dot{p}_f &= \frac{\partial \mathcal{H}}{\partial q_f} = \omega_0 q_f + G_- q_a \sqrt{1 - \frac{q_a^2 + p_a^2}{4J}} .
\end{aligned} \tag{11}$$

It is important to note the restriction in energy to be shared in the classical counterpart of the atomic degree of freedom, i.e.,

$$p_a^2 + q_a^2 \leq 4J. \tag{12}$$

This represents a fundamental difference between these two degrees of freedom. From the quantum point of view, the atomic degree of freedom is associated to a finite dimensional Hilbert space whereas the harmonic oscillator to a Hilbert space of infinite dimension.

Except when otherwise noted, in all cases to be presented here the parameter values we chose are $J = 9/2$, $G = 0.5$ and $G' = 0.2$, and $\varepsilon = \omega_0 = 1$ (as shown in Ref. [18], for these parameter values the nearest neighbor distribution of the energy level spacings is of a GOE type). For the classical Hamiltonian in eq. (10) we chose an energy value $E = 8.5$ for which the Poincaré section ($q_f = 0$) is shown in Fig. 1a. Note the presence of two islands, one of them of considerable relative size. In the center of such islands are located the two shortest stable periodic orbits whose atomic projections are shown in Fig. 1b. The symbols in the Poincaré section (Fig. 1a) represent the center of the initial quantum wave packets whose time evolution we will show in the next section. For the sake of comparison we also study the classical energy $E = 35$ whose Poincaré section is shown in Fig. 2a. The size of the many regular islands is comparatively much smaller. Both chosen energies are larger than the limit given by eq. (12), therefore the entire atomic phase space is energetically available for all initial conditions in the Poincaré sections. Moreover, the fact that the energies are large enough together with the limitation imposed by eq. (12) have dramatic consequences on the form

of the projections of the periodic orbits onto the atomic phase space. One can see an example of this in Fig. 2b (this particular point has been explored in Refs. [17, 19]).

III ENTANGLEMENT DYNAMICS IN REGULAR REGIONS

The linear entropy $\delta(t)$ corresponding to the reduced density matrix for the atomic subsystem is shown in Fig. 3a for initial conditions of the type given in eq. (4), where the center of these wave packets are on the periodic orbits indicated in Fig. 1a. Note that the linear entropy not only increases but exhibits a well marked oscillatory behavior, indicating that the system recovers coherence in a periodic way, for sufficiently short times. Interestingly enough, however, the period of recoherences observed in the linear entropy do **not** correspond to the period τ of the periodic orbit in question. It is **smaller**, roughly $\tau/2$. This indicates that another property of these orbits may be playing a role. This property is the **shape** of the spin (atomic) projection of the orbit. Note the strong correlation between the maximum growth in linear entropy and the closest approach to the classical atomic phase space border. This happens in the cases shown here and in all cases we analyzed, for short enough times. A natural question arises as to the representation dependence of our explanation. In order to clarify this point we use a representation independent quantity which is intimately connected to the radius of the orbit projection, the expectation value of the operator J_z [20]. In Fig. 3a we also show $\frac{d\delta}{dt}$ and $Tr(J_z\rho_a(t))$. Note that the first four maxima in $\langle J_z \rangle(t)$ correspond to a very good accuracy to maxima in $\frac{d\delta}{dt}$, indicating that whenever the “radius” is maximum, a maximum growth in linear entropy is found. It is in this sense that we conclude that the recoherences, purity gains found in the time evolution of quantum coherent wave packets initially centered at the regular region, are related to the proximity of the classical atomic phase space border. Of course when the initial wave packet is centered on a periodic orbit located in a smaller island, as is the case of the second orbit in Fig. 1b, the chaotic vicinities also play an important role and the established connection between $\frac{d\delta}{dt}$ and $Tr(J_z\rho_a(t))$ is less pronounced, as shown in Fig. 3b. Due to the shape of the orbit, in this case the proximity to the center and hence the minima of both functions are more clearly seen

to be connected. We next consider two more cases which independently corroborate these findings. Consider first the Poincaré section in Fig. 2a and the initial condition for the quantum evolution centered at the circle marked in the section, and the spin projection of the periodic orbit shown in Fig. 2b. In this case we note that the amount of time spent in the vicinities of the phase space border (performing the “loop” in Fig. 2b) is large compared to the period of the orbit. Note that during this time, $\frac{d\delta}{dt}$ is positive and the linear entropy grows (see Fig. 3c). Also, for the subsequent times where the orbit quickly crosses from one “loop” to the other, it approaches the center of the atomic phase space and correspondingly $\frac{d\delta}{dt}$ becomes negative and the linear entropy decreases. Since the time of growth is much larger than the one of decreasing, the linear entropy reaches the plateau faster.

On the other hand, in the integrable case $G' = 0$, the spin (atomic) projection of the periodic orbits are circular. In this case, if the argument is valid, one should expect no oscillations in $\delta(t)$. This is in fact the case, as shown in Fig. 4 where one sees, moreover, that it takes a longer time for the linear entropy to reach the plateau, due to the considerable (and constant) distance between the orbit and the atomic phase space border.

IV ENTANGLEMENT DYNAMICS IN THE CHAOTIC REGION

As discussed in Ref. [6] the entanglement in the chaotic region is in general faster than in the regular region. In Fig. 5a we show the idempotency defect (linear entropy) for the initial conditions of the form (4) centered at the triangles marked on the Poincaré section of Fig. 1a, and in Fig. 5b the projection of the orbits for the specific cases of the initial conditions labeled c_1 and c_2 (see figure captions). In these cases the linear entropy does not exhibit periodic oscillations, albeit oscillations are still present. Although they are not directly related to a periodic orbit, one can explain the oscillations very much along the lines followed in the regular case. If we take a classical trajectory associated with the center of the wave packet and follow its projection on the atomic phase space, we notice again that the proximity of this phase space border plays a decisive role on the decoherence process. This is illustrated in Figs. 5c and 5d for the initial conditions c_1 and c_2 . For the case c_2 , decoherence is retarded due to the fact that the wave packet moves ini-

tially towards the center of the phase space, following the classical trajectory shown in Fig. 5b. Note that as soon as the classical trajectory approaches the border there is a corresponding increase in the entanglement rate $\frac{d\delta}{dt}$ in Fig. 5d. Thus the linear entropy increases. In terms of the representation independent quantity $\langle J_z \rangle(t)$, the same features prevail. The remaining initial condition c_3 for which $\delta(t)$ has been evaluated in Fig. 5a behaves in qualitatively analogous way, as for instance the trajectory labeled c_1 shown in Fig. 5b, and will not be shown here. As to be expected, in the chaotic region the relation between the motion of the quantum wave packet and the classical trajectory associated to its center is rapidly overwhelmed by other effects such as the rapid spreading of the quantum wave function. In fact, in Fig. 6 we show the time evolution of the spin Husimi distribution associated with the initial condition c_2 in Fig. 5. This figure illustrates the given argument. Moreover, we see that for times when the plateau in $\delta(t)$ is reached, the spin Husimi distribution is totally delocalized in the corresponding phase space. Finally we note that this is not a characteristic of the chaotic initial condition; the wave packets centered at regular initial conditions also become spread all over the spin phase space by the time the linear entropy reaches the plateau.

V SUMMARY

The present work has been devoted to a detailed analysis of the dynamics of the process of entanglement in the chaotic N -atom Jaynes-Cummings model. Previous work on the model [6, 21] pointed out general features of the process, mainly focusing on differences between chaotic and regular regimes (unstable and stable). The entanglement process of the model is however very rich and much more can be learned from specific features of the linear entropy such as its oscillations (recoherences in time, periodic or not). We have found an intimate connection between these recoherences and classical orbits. Specifically, we have pointed out the very special role played by the morphology of the spin-projected classical orbits. This is in accordance with the known fact that the decoherence properties are dictated by the smaller subsystem [22].

Considering the present state of experimental proposals and realizations of atomic coherent states in the N -atom JCM, it seems that the integrable RW case ($G' = 0$) is more likely to be realizable in a practical implementation

of the model considered in this work. Although not shown here, the RW case was checked for regular initial conditions on tori in phase space and showed similar recoherence phenomena, as described in the previous sections.

Despite the fact that these findings are model dependent, we believe them to be typical of systems involving two degrees of freedom, one of them having a Hilbert space with dimension much greater than the dimension of the other, and whose classical limit is chaotic (soft chaos).

Acknowledgements

It is a pleasure to thank Prof. H. A. Weidenmüller for first calling our attention to the need to explain the oscillations in the linear entropy, and T. H. Seligman for helpful discussions and for reading the manuscript. The authors acknowledge financial support to the Brazilian agencies Fundação de Amparo à Pesquisa do Estado de São Paulo (FAPESP) and Conselho Nacional de Desenvolvimento Científico e Tecnológico (CNPq).

References

- [1] Letter from Albert Einstein to Max Born in 1954, cited by E. Joos, in *New Techniques and Ideas in Quantum Measurement Theory*, edited by D. M. Greenberger (New York Academy of Science, New York, 1986).
- [2] H. D. Zeh, *Found. Phys.* **1**, 69 (1970); H. Dekker, *Phys. Rev. A* **16**, 2126 (1977); W. H. Zurek, *Phys. Rev. D* **24**, 1516 (1981); **26**, 1862 (1982); W. G. Unruh and W. H. Zurek, *ibid.* **40**, 1071 (1989); W. H. Zurek, *Phys. Today* **44**, 36 (1991); B. L. Hu, J. P. Paz, and Y. Zhang, *Phys. Rev. D* **45**, 2843 (1992); W. H. Zurek, S. Habib, and J. P. Paz, *Phys. Rev. Lett.* **70**, 1187 (1993); D. Giulini, E. Joos, C. Kiefer, J. Kupsch, I. O. Stamatescu, and H. D. Zeh, *Decoherence and the Appearance of a Classical World in Quantum Theory* (Springer-Verlag, Berlin, 1996).
- [3] M. Brune, E. Hagley, J. Dreyer, X. Maître, A. Maali, C. Wunderlich, J. M. Raimond, and S. Haroche, *Phys. Rev. Lett.* **77**, 4887 (1996); C. Monroe, D. M. Meekhof, B. E. King, and D. J. Wineland, *Science* **272**, 1131 (1996).
- [4] W. H. Zurek and J. P. Paz, *Physica (Amsterdam)* **83D**, 300 (1995); W. H. Zurek, S. Habib, and J. P. Paz, *Phys. Rev. Lett.* **70**, 1187 (1993).
- [5] A. Tameshtit and J. E. Sipe, *Phys. Rev. A* **47**, 1697 (1993); K. Shiokawa and B. L. Hu, *Phys. Rev. E* **52**, 2497 (1995).
- [6] K. Furuya, M. C. Nemes, and G. Q. Pellegrino, *Phys. Rev. Lett.* **80**, 5524 (1998).
- [7] M. Tavis and F. W. Cummings, *Phys. Rev.* **170**, 379 (1968); see also R. H. Dicke, *ibid.* **93**, 99 (1954).
- [8] G. S. Agarwal, R. R. Puri and R. P. Singh, *Phys. Rev. A* **56**, 2249 (1997); C. C. Gerry and R. Grobe, *ibid.* **56**, 2390 (1997); **57**, 2247 (1998); M. G. Benedict and A. Czirják, *ibid.* **60**, 4034 (1999).
- [9] J. Recamier, O. Castañós, R. Jáuregui, and A. Frank, *Phys. Rev. A* **61**, 063808 (2000).
- [10] A. Rauschenbeutel, G. Nogues, S. Osnaghi, P. Bertet, M. Brune, J.-M. Raimond, and S. Haroche, *Science* **288**, 2024 (2000).

- [11] K. Mølmer and A. Sørensen, Phys. Rev. Lett. **82**, 1835 (1999); A. Sørensen and K. Mølmer, Phys. Rev. A **62**, 022311 (2000).
- [12] Q. A. Turchette, C. S. Wood, B. E. King, C. J. Myatt, D. Leibfried, W. M. Itano, C. Monroe, and D. J. Wineland, Phys. Rev. Lett. **81**, 3631 (1998); C. A. Sackett, D. Kielpinski, B. E. King, C. Langer, V. Meyer, C. J. Myatt, M. Rowe, Q. A. Turchette, W. M. Itano, D. J. Wineland, and C. Monroe, Nature (London) **404**, 256 (2000).
- [13] Ch. Roos, Th. Zeiger, H. Rohde, H. C. Nägerl, J. Eschner, D. Leibfried, F. Schmidt-Kaler, and R. Blatt, Phys. Rev. Lett. **83**, 4713 (1999).
- [14] J. I. Cirac, A. S. Parkins, R. Blatt, and P. Zoller, Adv. Atom. Mol. Phys. **37**, 237 (1996).
- [15] P. W. Milonni, J. R. Ackerhalt and H. W. Galbraith, Phys. Rev. Lett. **50**, 966 (1983); P. W. Milonni, M. L. Shih and J. R. Ackerhalt, *Chaos in Laser-Matter Interactions*, World Scientific Lecture Notes in Physics Vol.6 (World Scientific, Singapore, 1987); R. Graham and M. Höhnerbach, Z. Phys. B **57**, 233 (1984); idem in *Quantum Measurement and Chaos*, edited by E. R. Pike and S. Sarkar, NATO Advanced Study Institute, Series B, Vol. 161, (Plenum, New York, 1987), p. 147.
- [16] J. R. Klauder and B.-S. Skagerstam, *Coherent States: Applications in Physics and Mathematical Physics* (World Scientific, Singapore, 1985).
- [17] M. A. M. de Aguiar, K. Furuya, C. H. Lewenkopf, and M. C. Nemes, Ann. Phys. **216**, 291 (1992).
- [18] C. H. Lewenkopf, M. C. Nemes, V. Marvulle, M. P. Pato, and W. F. Wreszinski, Phys. Lett. A **155**, 113 (1991).
- [19] M. A. M de Aguiar, K. Furuya, C. H. Lewenkopf, and M. C. Nemes, Europhys. Lett. **15**, 125 (1991); K. Furuya, M. A. M de Aguiar, C. H. Lewenkopf, and M. C. Nemes, Ann. Phys. **216**, 313 (1992).
- [20] This connection is easily seen by noting that $\langle wv | J_z | wv \rangle = \frac{1}{2}(p_a^2 + q_a^2 - 2J)$.
- [21] R. M. Angelo, K. Furuya, M. C. Nemes, and G. Q. Pellegrino, Phys. Rev. E **60**, 5407 (1999).

- [22] E. Schrödinger, Proc. Phil. Soc. **31**, 555 (1935); **32**, 446 (1936); M. C. Nemes and A. F. R. de Toledo Piza, Physica A **137**, 367 (1986); A. Ekert and P. L. Knight, Am. J. Phys. **63**, 415 (1995).

Figure Captions

Figure 1: **(a)** Poincaré section given by $q_f = 0.0$ and $p_f > 0.0$ for the spin degree of freedom with $J = 9/2$ in the nonintegrable ($G = 0.5$ and $G' = 0.2$) and resonant ($\varepsilon = w_0 = 1$) case — these values will be the same in all subsequent figures except when otherwise noted. Here we show the section for the energy $E = 8.5$. The marks represent the various choices for the center of the coherent states: circles for regular initial conditions (IC) and triangles for chaotic ones. **(b)** Spin projection of the two shortest stable periodic orbits indicated by circles in (a) (the border line is also shown). Initial conditions at the surface of section are as follows: ($q_a = 0.0, p_a = 2.261, q_f = 0.0, p_f = 3.423276$) for the first (elliptic) orbit with period $\tau = 4.89$; ($q_a = 0.0, p_a = -3.577, q_f = 0.0, p_f = 5.221656$) for the second orbit with period $\tau = 7.45$.

Figure 2: **(a)** Poincaré section for the energy $E = 35$. The circle represents the center of the coherent state for one regular initial condition. **(b)** Spin projection of the shortest stable periodic orbit, indicated by the circle in (a). Initial condition at the surface of section is as follows: ($q_a = 0.0, p_a = 1.4175, q_f = 0.0, p_f = 7.888904$) with period $\tau = 5.82$.

Figure 3: Linear entropy $\delta(t)$ (continuous lines), its derivative $\frac{d\delta(t)}{dt}$ (dashed lines), and the normalized expectation value $\langle J_z \rangle(t)/J$ (dot-dashed lines) as functions of time. **(a)** for the first regular initial condition of Fig. 1b. Note the correspondence between the maxima and minima of $\frac{d\delta(t)}{dt}$ and $\langle J_z \rangle(t)/J$. **(b)** for the second regular initial condition of Fig. 1b. In this case, only the minima of $\frac{d\delta(t)}{dt}$ and $\langle J_z \rangle(t)/J$ have a clear correspondence due to the peculiar form of the orbit (see second figure of Fig. 1b). **(c)** Regular initial condition as marked in Fig. 2a and its spin-projected orbit shown in Fig. 2b; during the interval of time corresponding to the rise of $\delta(t)$ there is an approximate correspondence between the maxima and minima of $\frac{d\delta(t)}{dt}$ and those of $\langle J_z \rangle(t)/J$.

Figure 4: For the energy $E = 8.5$ in the integrable ($G = 0.5$ and $G' = 0.0$) and resonant ($\varepsilon = w_0 = 1$) case, the plot of linear entropy $\delta(t)$ for initial condition on a periodic orbit which is **circular** (see inset) ($q_a = 0.0, p_a = 2.47675, q_f = 0.0, p_f = 3.563642$). Notice that the curve shows practically no oscillations as compared to Fig. 3a.

Figure 5: **(a)** Linear entropy $\delta(t)$ for the **chaotic initial conditions** corresponding to the triangles shown in Fig. 1a: c_1 ($q_a = -4.0, p_a = 0.0, q_f = 0.0, p_f = 3.162278$) for the continuous line; c_2 ($q_a = 1.57, p_a = -2.0, q_f = 0.0, p_f = 5.680465$) for the dashed line; and c_3 ($q_a = 3.0, p_a = 2.0, q_f = 0.0, p_f = 2.942413$) for the dot-dashed line. **(b)** Spin projections of the orbits c_1 and c_2 . Various times are indicated along the orbits showing that the initial conditions are such that the trajectory c_2 in spin phase space is launched inward as opposite to the case c_1 for instance. **(c)** $\delta(t)$ (continuous line), $\frac{d\delta(t)}{dt}$ (dashed line), and $\langle J_z \rangle(t)/J$ (dot-dashed line) for c_1 . **(d)** $\delta(t)$ (continuous line), $\frac{d\delta(t)}{dt}$ (dashed line), and $\langle J_z \rangle(t)/J$ (dot-dashed line) for c_2 . During the interval of time corresponding to the rise of $\delta(t)$ there is an approximate correspondence between the maxima and minima of $\frac{d\delta(t)}{dt}$ and $\langle J_z \rangle(t)/J$ but for shorter time than it happens for the regular cases shown in Figs. 3a and 3b.

Figure 6: Spin Husimi distribution of the quantum coherent state initially centered at condition c_2 in Fig. 5. Snapshots are taken at time values $t = 0$ (upper left), $t = 1$ (upper right), $t = 4$ (down left), and $t = 25$.

This figure "Fig1a.jpeg" is available in "jpeg" format from:

<http://arxiv.org/ps/quant-ph/0106118v1>

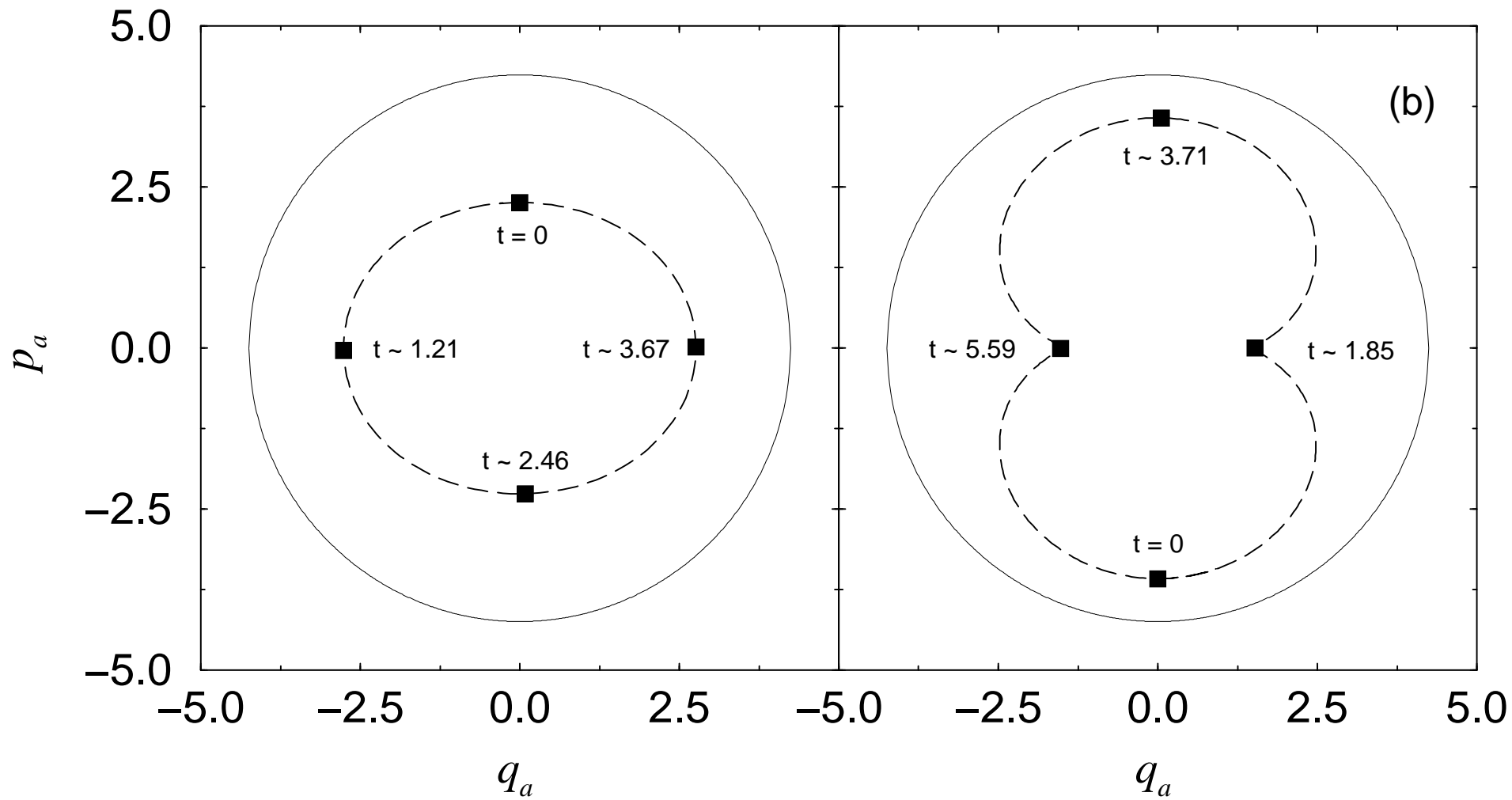


Fig. 1b

This figure "Fig2a.jpeg" is available in "jpeg" format from:

<http://arxiv.org/ps/quant-ph/0106118v1>

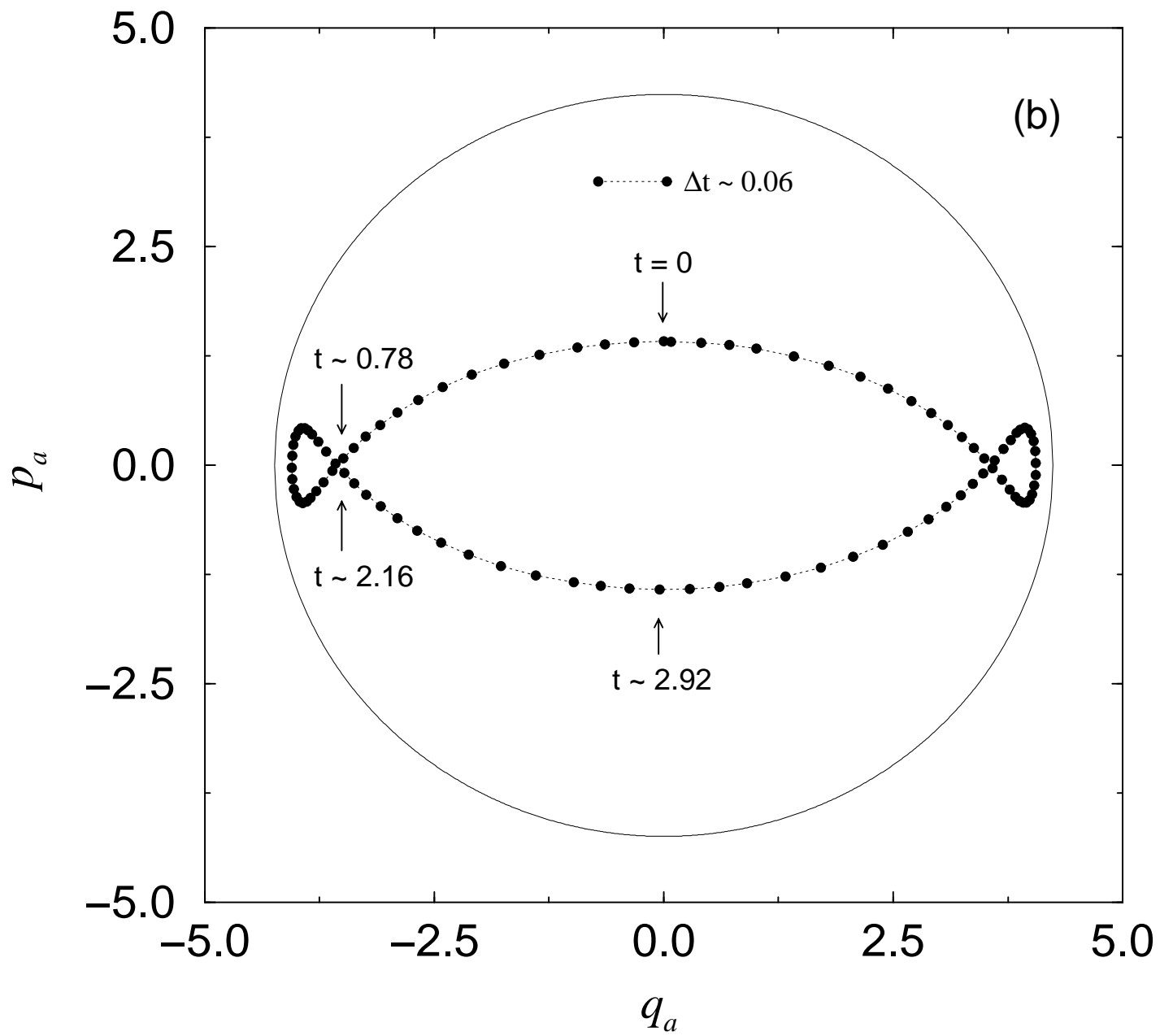


Fig. 2b

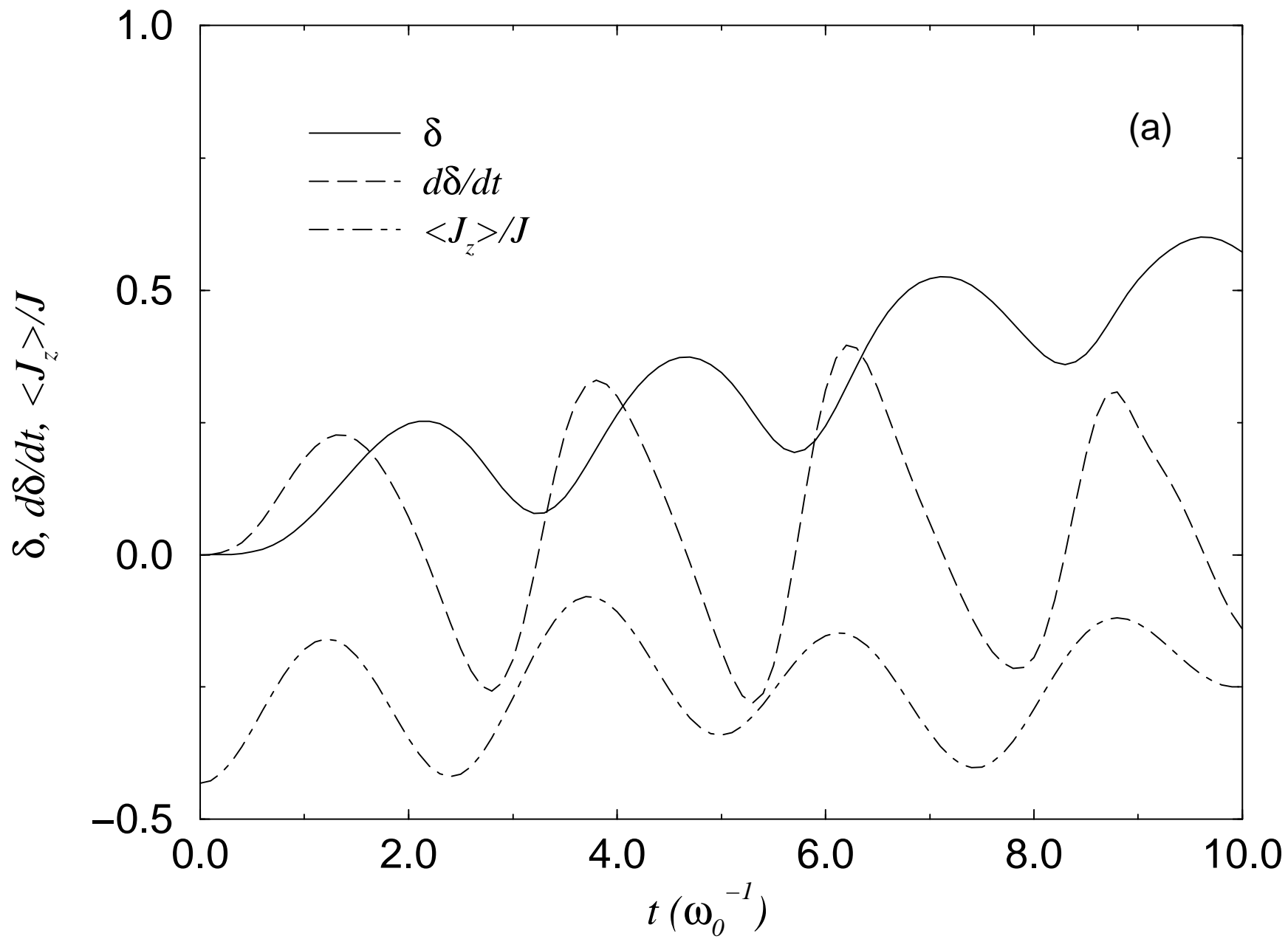


Fig. 3a

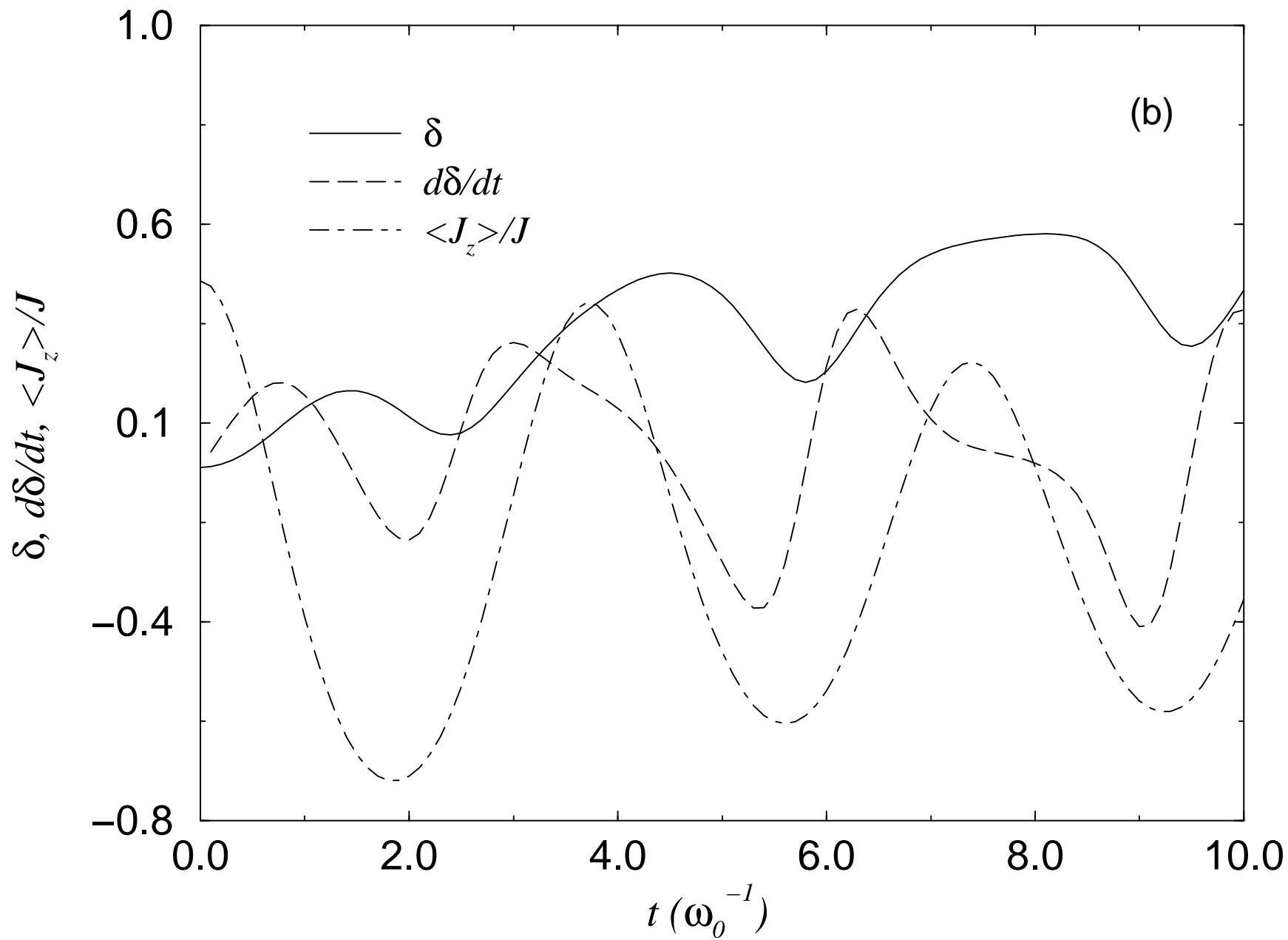


Fig. 3b

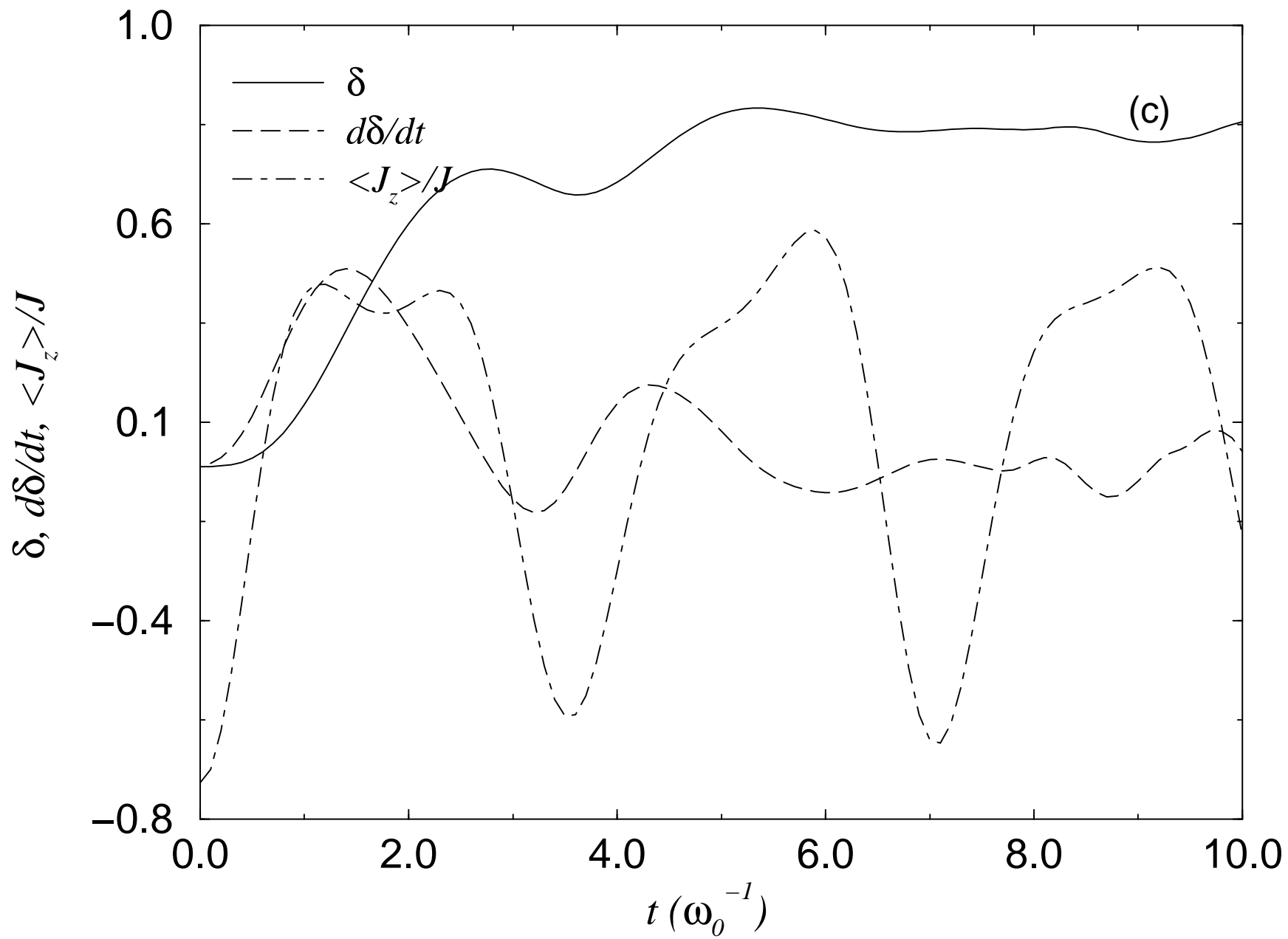


Fig. 3c

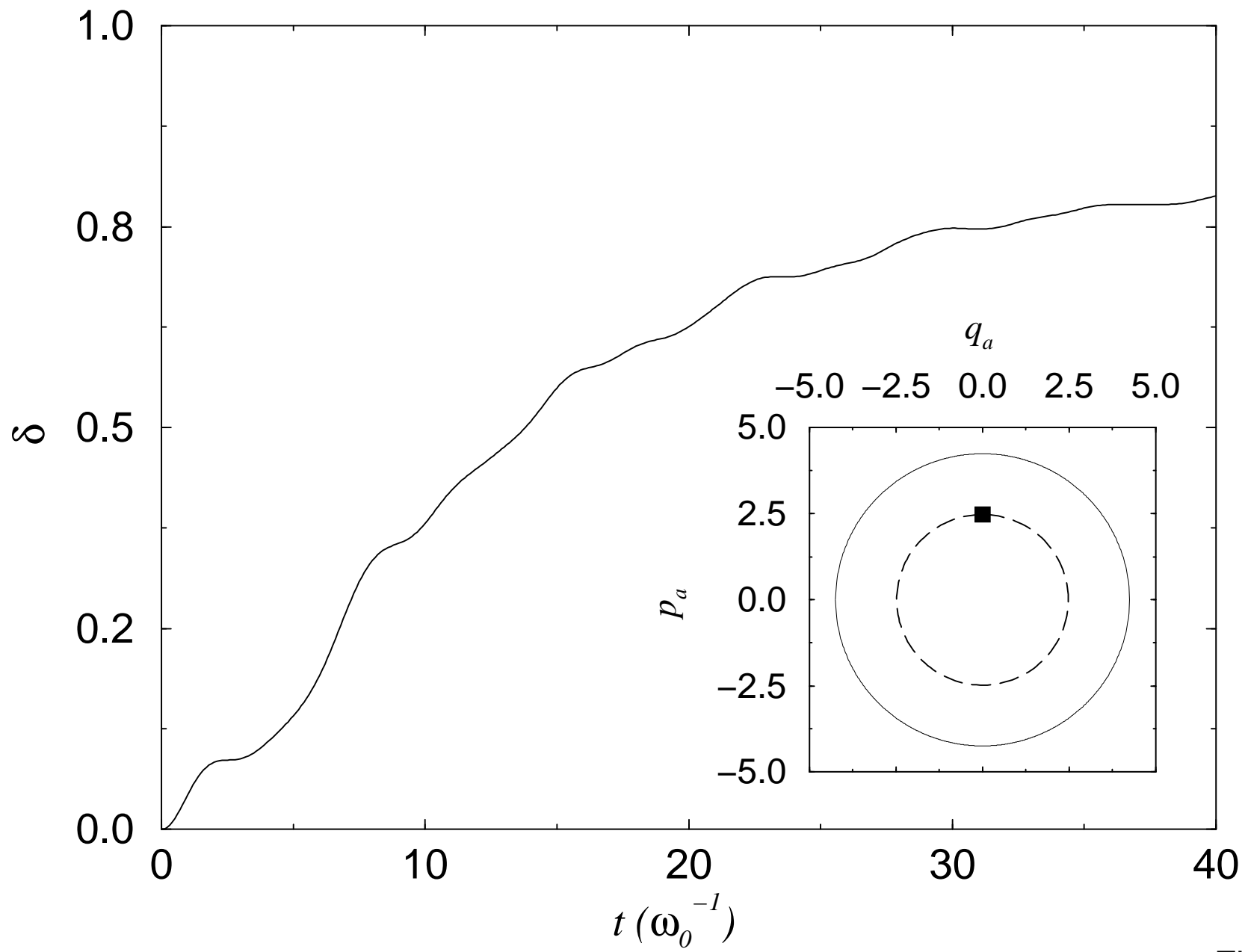


Fig. 4

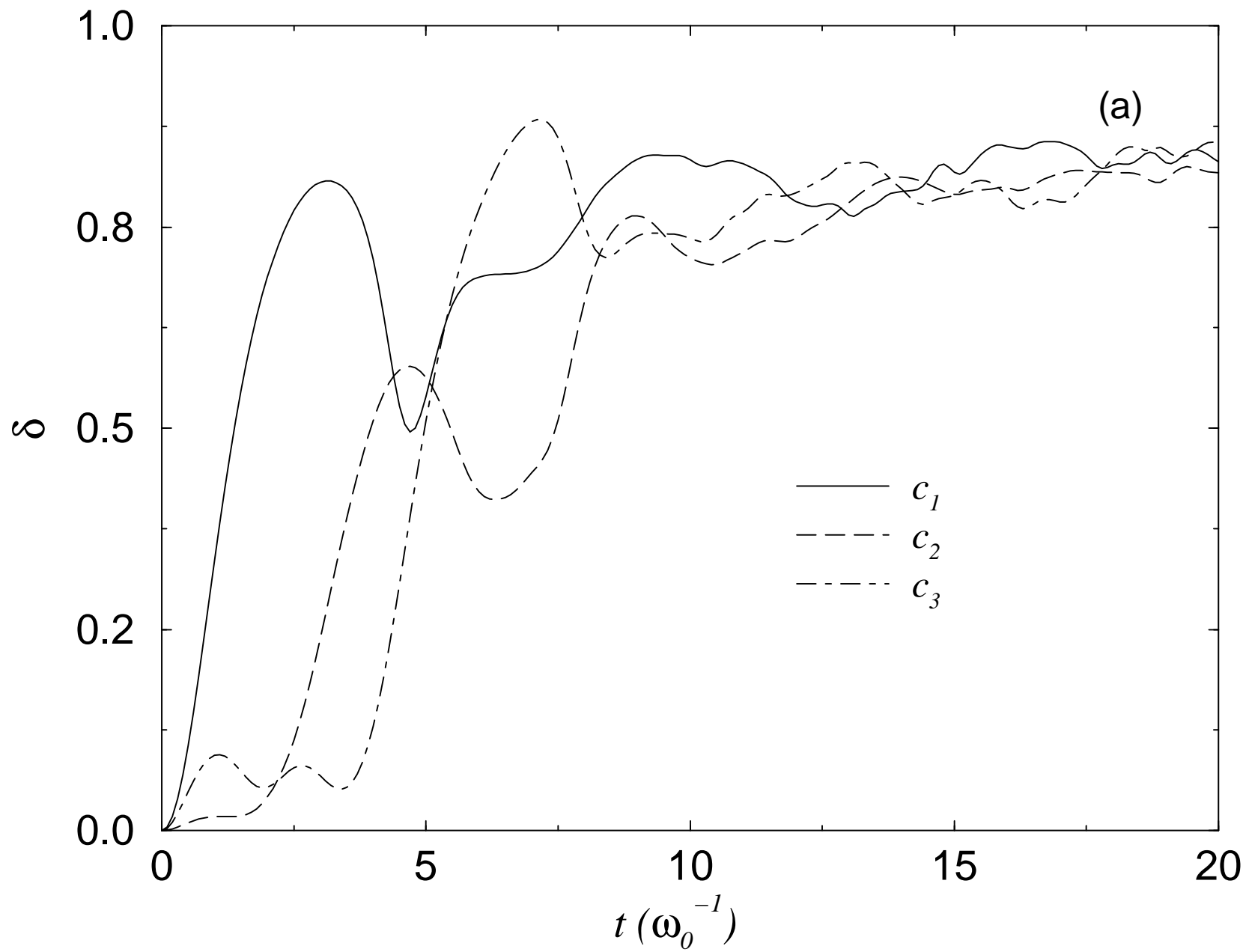


Fig. 5a

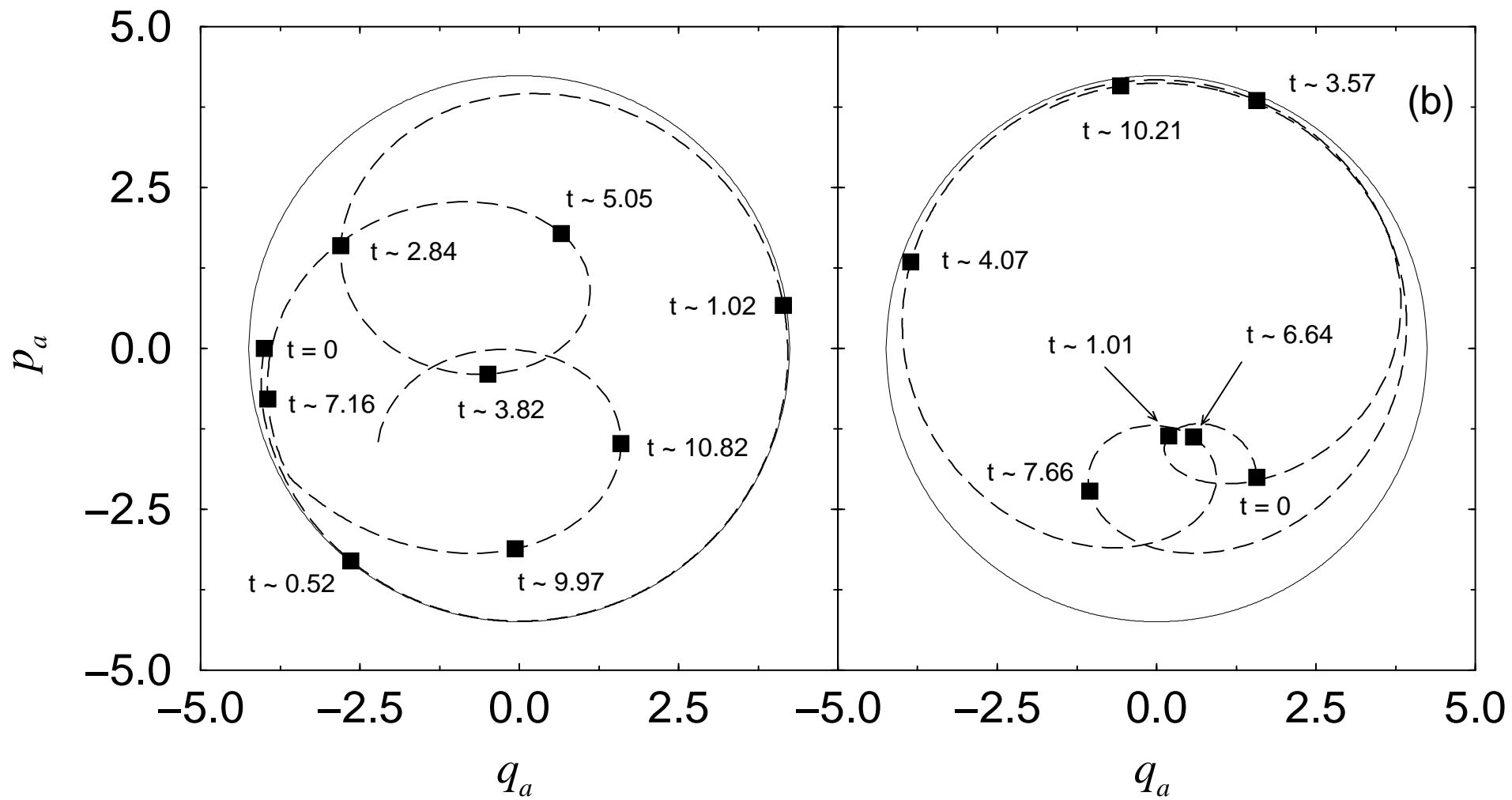


Fig. 5b

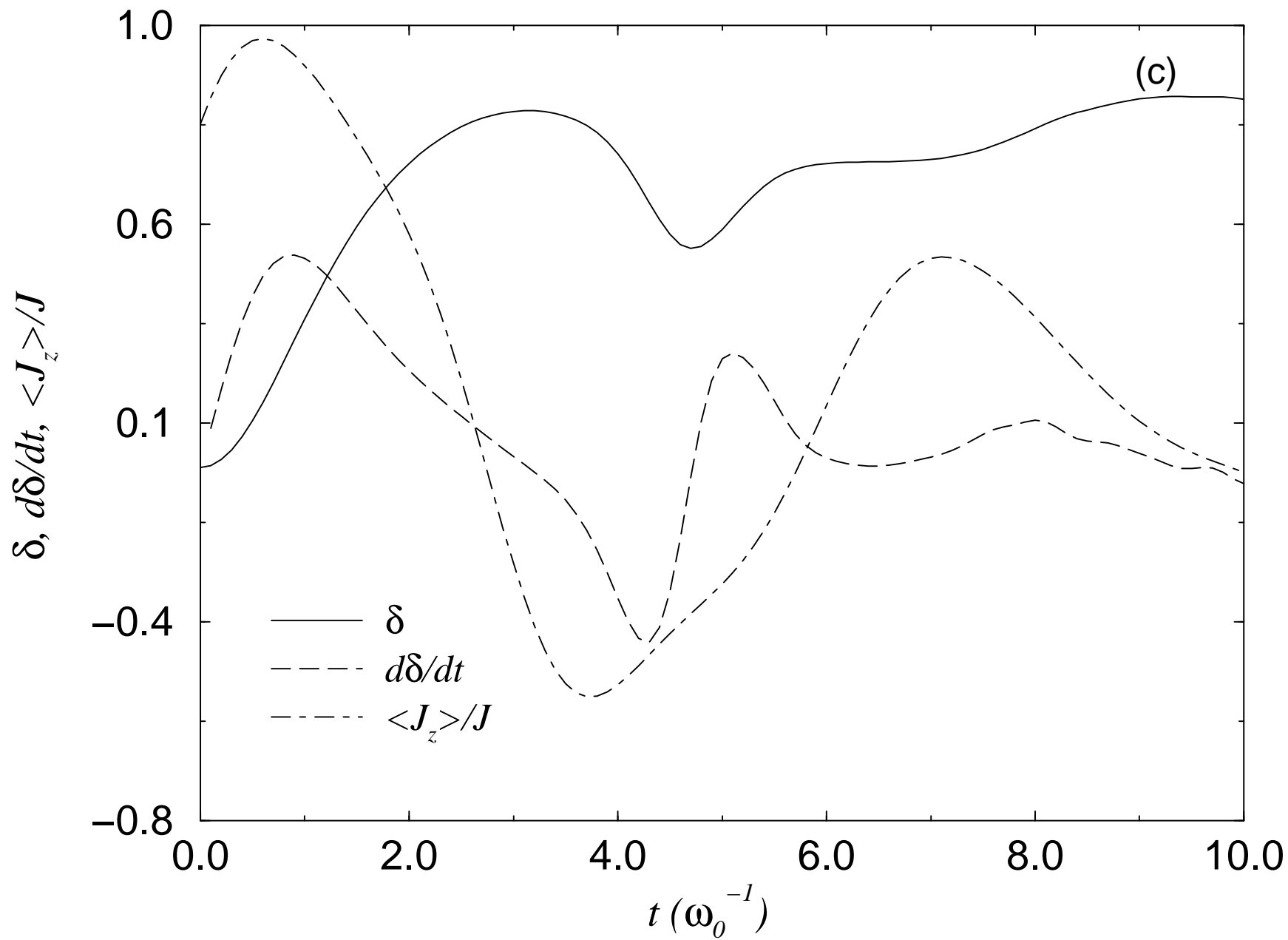


Fig. 5c

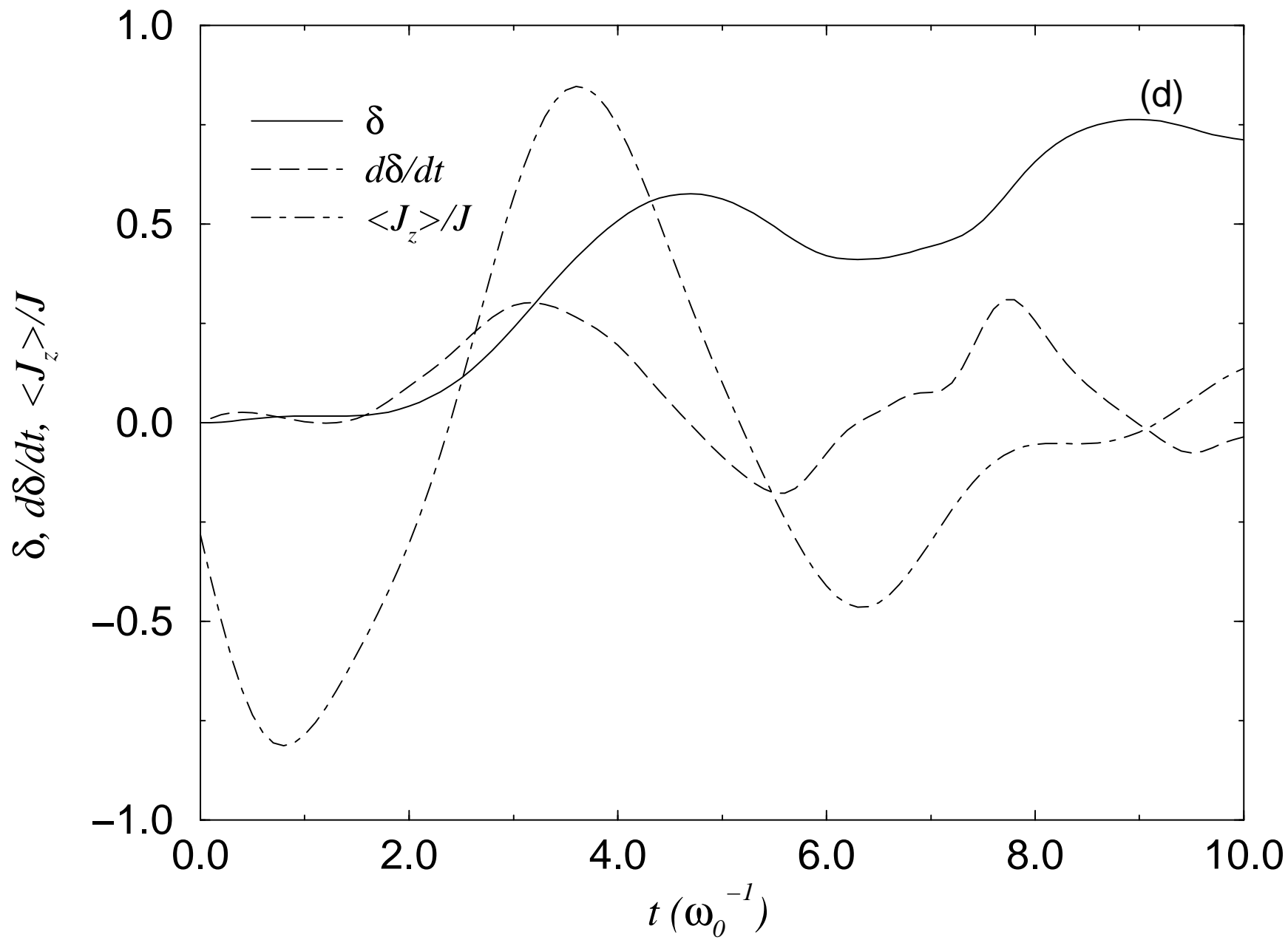


Fig. 5d

